Lawrence Berkeley National Laboratory

Title

Metal—ceramic composite structures for fabrication of high power density plasmonic devices

Authors

Otto, Lauren M
Liu, Stephanie E
Ng, Rowena W
et al.

Peer reviewed

Metal–ceramic composite structures for fabrication of high power density plasmonic devices ⊘

Lauren M. Otto ✉ ⓘ ; Stephanie E. Liu; Rowena W. Ng; Adam M. Schwartzberg; Shaul Aloni; Aeron Tynes Hammack ⓘ

Check for updates

View Online   Export Citation   CrossMark

Journal of Applied Physics

Special Topic: Phase-change Materials and Their Applications

Submit Today

AIP Publishing

AIP Publishing

Metal–ceramic composite structures for fabrication of high power density plasmonic devices

View Online   Export Citation   CrossMark

Lauren M. Otto,[1,2,a]   Stephanie E. Liu,[1,2,3] Rowena W. Ng,[1,2] Adam M. Schwartzberg,[2] Shaul Aloni,[2]
and Aeron Tynes Hammack[1,2]

AFFILIATIONS

[1]Laminera LLC, Berkeley, California 94703, USA

[2]Molecular Foundry, Lawrence Berkeley National Laboratory, Berkeley, California 94720, USA

[3]Department of Materials Science and Engineering, University of California, Berkeley, California 94720, USA

Note: This paper is part of the Special Collection Recognizing Women in Applied Physics.
[a]**Author to whom correspondence should be addressed:** lauren@laminera.io

ABSTRACT

The recent decade brought many advances to plasmonics, but high power density plasmonic antennas designed to behave as heaters or operate in high temperature environments are still facing material stability challenges preventing their ultimate use. Gold has been the optimal choice among plasmonic materials but experiences morphology changes at temperature that result in device efficiency reduction and failure. Bulk titanium nitride has been explored as a solution but has deal-breaking tradeoffs in device quality factor. In this paper, we explore via proof-of-concept the use of a metal–ceramic composite structure to determine whether a bulk Au nanorod can provide strong plasmonic resonances while coated with an ultrathin conformal layer of titanium nitride or silica to provide morphological stability and sufficient plasmonic activity without excessive resonance quality degradation. We show SEM-level morphological stability for temperatures up to 500 °C with coatings below 4 nm. Computer modeling suggests the ultrathin titanium nitride has detrimental effects on the strong plasmonic resonances of a Au nanorod. We then looked into other possible coatings for solutions to stabilize high power density plasmonic antennas including plasmonic oxides, metal adhesion layers, and silica, the latter appearing to be the best option while lowering the overall peak electric field intensity, the silica increases the electric field intensity at its boundary.

INTRODUCTION

Plasmonic technologies have seen significant advancement over the last decade, but the sub-category of high power density plasmonic devices like those used for nonlinear optical effects[1–3] and nanoscale heating and light focusing, such as the heat-assisted magnetic recording (HAMR) technology,[4–6] is still facing thermal instability issues with common solutions bringing unwanted trade-offs in device quality factors (e.g., resonance strength and full width at half maximum, lifetime, thermal conduction, etc.).[1–3] Particularly for HAMR technology in future hard disk drives (HDDs), the plasmonic antenna is precisely defined to nanofocus ~810–830 nm light from a laser and photonic waveguide to a 10 s of nanometers spot size on the magnetic media where the bit is then recorded only in the heated spot where the magnetic coercivity is now small enough for manipulation by the magnetic write

pole in the HDD's head.[4,5] During recording, the magnetic media could see a temperature increase of ~500 °C[7] with the plasmonic antenna itself seeing at least a ~100–200 °C temperature increase,[8] if not closer to 400 °C,[2] which is enough to cause surface diffusion and deformation of the Au used to make the plasmonic antenna.[9,10] When deformed over time, the plasmonic antenna no longer maintains its designed morphology and no longer performs optimally, leading to head and drive failure.[1] The HDD industry and academic researchers have explored many possibilities for solving this reliability challenge, which have included investigating many Au–metal alloys[9,10] exploring adhesive layers,[11,12] and testing refractory metals such as titanium nitride for their thermal stability benefits,[13] each carrying their own tradeoff with the problem at hand and the need for Au's efficiency in far-field to near-field conversion and chemical stability among other adjacent materials challenges.[1–3] TiN has received much attention from academic

groups, and its development focused on bulk structures with high plasmonic figure of merit (FOM = $-\epsilon'_m/\epsilon''_m$, the negative ratio of the real to imaginary parts of the material's dielectric function, which represents its ability to host a surface density wave of electrons known as a plasmon).[1,13–21] Unfortunately, TiN has a much lower FOM than Au (<5 vs >15, respectively, near ~810–830 nm),[15,22,23] which hurts its chances as a bulk material candidate, and TiN's thermal conductivity is >10× less than Au meaning that its use as a bulk plasmonic structure will cause the HAMR antenna (or other antenna structures) to heat up *more* and make the thermal problems in the HDD head worse and not better. Furthermore, the common method used to derive such high-quality TiN (sputtering) was performed at temperatures in excess of 600 °C,[16,18] which is far outside of the thermal tolerance of HDD head manufacturing that requires deposition temperatures below 200–300 °C for maintenance of the tunneling magnetoresistive read sensors.[24] For these reasons, we chose to explore the use of TiN as an ultrathin (<7 nm) coating to optimize for the maximum amount of bulk Au in the plasmonic antenna for the possible added benefits of the exterior thermal stability of TiN in place to define the antenna's precisely designed shape. We also chose to form the conformal and ultrathin TiN films using low-temperature plasma-enhanced atomic layer deposition (PEALD), a scalable industrial technique, for use in HAMR head fabrication. In this paper, we review the concept of our metal–ceramic composite plasmonic structure, outline methods for test fabrication, demonstrate proof-of-concept for the structural stability of the composite structure under thermal treatments, discuss modeling results for TiN layer application and design, and discuss further methods for improvement and continued research.

We chose to perform preliminary proof-of-concept tests on the structural stability of TiN-coated Au plasmonic nanorods [Figs. 1(a) vs 1(b)] with the expectation that even a modest coating of TiN would yield noticeable benefits. We used silicon wafer coupons (silicon with native oxide) as substrates for the Au nanorods, which were applied following a solution of positively charged poly-L-lysine that was deposited to promote electrostatic adhesion of the nanorods to the surface of the coupons [Fig. 1(c)].[25] The nanorods were then added, and the majority of the coupons were coated in layers of TiN varying in thickness (0.43, 1.0, 1.5, 2.0, and 3.9 nm) using PEALD at 90 °C, which was chosen for two reasons. First, it has been noted that Au softening can occur at only 100 °C,[9] and second prior work from the authors has shown that the 90 °C PEALD TiN in this work can be better annealed into a crystalline structure than higher temperature (~200 °C) TiN.[26] Depending on the thermal budget of a plasmonic structure and its containing device, higher temperature or additional thermal processing could be tolerated. Furthermore, the plasmonic structure itself could be used to perform localized annealing of its surroundings to improve an outside film to the desired quality. Finally, it should be noted that upon exposure to air, TiN develops a native oxide that is 1–2 nm thick and composed of titania or $TiON_x$, after removal from the PEALD tool and prior to other experimental work.

Following PEALD deposition, the coated and uncoated Au nanorods were subjected to thermal annealing in a controlled argon environment for 0.5 h at 100, 200, 300, 400, and 500 °C to scan a relevant thermal energy range for a high power density
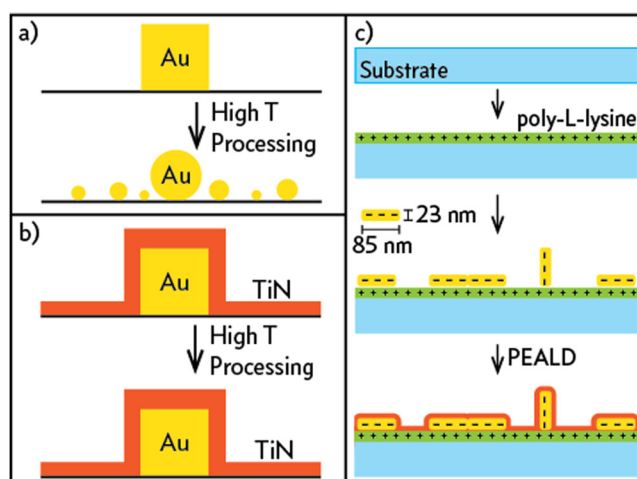

FIG. 1. An illustration of the concept of this work where a Au structure sits on a surface without (a) and with (b) a TiN coating. Morphological change in the Au structure occurs in (a) where high temperature processing causes the Au to change shape (surface energy minimizes) but does not occur in (b) when surrounded by the TiN coating. (c) The method for making the concept illustrated in (b) where a substrate is coated with positively charged poly-L-lysine, Au nanorods, and PEALD TiN.

plasmonic device such as those found in HAMR heads. When exploring morphology changes as a subject of temperature, the uncoated Au nanorods showed deformation starting at the 200 °C anneal temperature held for 0.5 h [Fig. 2(a)]. While it may appear qualitatively that the 0.43 nm (roughly one monolayer) coating of TiN was sufficient to preserve many of the nanorods' shapes when annealed at 400 °C, true statistical and quantitative data were not obtained. Morphology stability continued to improve up to about the 2.0 nm coating for this condition [Fig. 2(b)]. Gold nanorods coated with 2.0 and 3.9 nm of TiN showed strong abilities to maintain their morphology under all of our annealing conditions at a relevant scale qualitatively measured by our scanning electron microscopy (SEM) system. Similar tests were also performed with SiO_2 PEALD coatings (4.9 nm) and show similar stability results [Fig. 2(a)]. While these results are encouraging, higher resolution transmission electron microscopy (TEM) images are shared by Kautzky and Blaber[2] and show nanoscale morphological changes in Au plasmonic antennas due to densification of the deposited Au at elevated temperatures, which is not represented by our use of Au nanorods and SEM imaging.

To further study our concept, we proceeded with proof-of-concept theoretical modeling to explore the plasmonic behavior of the metal–ceramic composite antenna. Finite-difference time-domain (FDTD) Lumerical software was used to model the Au nanorods on SiO_2 substrates with coatings of TiN varying in thickness, silica coatings for an alternate non-plasmonic "control" material that has dielectric behavior and not plasmonic behavior, and uncoated Au nanorods as an additional "control." Dielectric functions for the Au and the coating materials are included in Figs. 3(a) and 3(b) with the films exhibiting plasmonic behavior having a FOM = $-\epsilon'_m/\epsilon''_m$ included
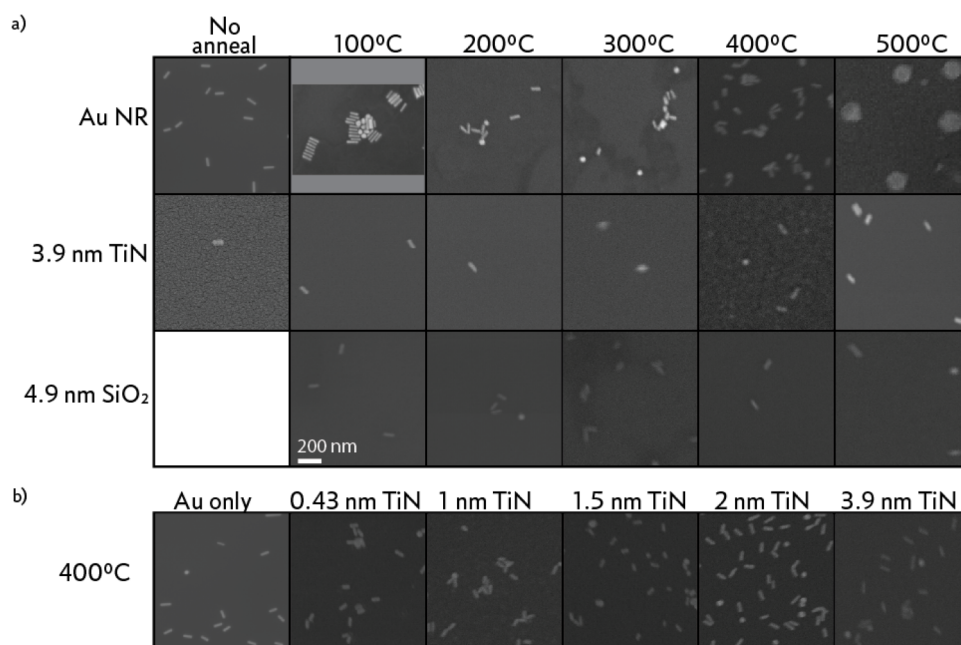
FIG. 2. (a) SEM images of bare and coated samples at annealing temperatures spanning 100–500 °C. There are clear morphological changes in bare Au nanostructures as low as 200 °C, whereas original rod morphology is preserved in systems with <4 nm TiN. (b) Deposition of various ultrathin TiN coatings was successful in preserving rod morphology at an annealing temperature of 400 °C for 30 min. All images are scaled to match the 200 nm scale bar.

in Fig. 3(c). Data for Au and Ag were taken from Johnson and Christy[22] and TiN when sputtered onto Al_2O_3 and MgO [1,2] were taken from Guler *et al.*[15] The remaining TiN materials were films we deposited with PEALD, measured with *in situ* spectroscopic ellipsometry, and fit using a Drude–Lorentz model to extract the pseudo-transformed dielectric function $\epsilon_m = \epsilon_m' + i\epsilon''$. The PEALD temperature used for depositing the room temperature modeled TiN is noted in the figure panels of Fig. 4(a). The thickness labeled (e.g., 2, 14 nm, thick, 90 or 300 °C deposited, etc.) is the film thickness where the thickness-dependent dielectric function is extracted from the model's fit of the *in situ* data, and "thick" corresponds to the film's full thickness, which is believed to be 216 nm; however, the thickness of an optically thick sample is hard to accurately measure with an optical technique. Both sets of data from TiN deposited at 300 °C are derived from the same film we previously published[6] and are included for a comparison with the ultrathin PEALD TiN films at 90 °C and the TiN films deposited by Guler *et al.*,[15] which we presume are optically thick. The TiN films from Guler *et al.* are modeled as a best-case scenario for TiN's plasmonic activity and our application in mind; however, the modeled performance with these data would be next to impossible to achieve given that the TiN quality when deposited on MgO is better due to lattice matching that will not occur on Au and because of the presumed TiN thickness that yields this high quality that is not present for ultrathin layers (see data for 300 °C TiN thick). Ag and Au 2 nm layers are modeled as a blue-shifting comparison. The modeled nanorod and coating configurations on the substrate are included in Fig. 3(d) and are further discussed in the Methods.

Specifically concerning the application of a plasmonic antenna as a far-field to near-field converting device with the desired implication of nanospot heating only a few nanometers from itself, such as what is found in a HAMR head, we were particularly interested in the local electric field intensity surrounding the coated Au nanorods. Basic surface plasmon sensor theory would suggest that a material like SiO_2 would simply red-shift the resonant frequency/wavelength of the Au nanorod and would also internally encapsulate the former maximum electric field intensity internally rendering it inaccessible for heating other nearby media. Conversely, we were hypothesizing that the plasmonic nature of the TiN could extend the plasmonic nature of the Au nanorod further into space allowing for the maximum electric field intensity to be external to the coating and remain accessible for near-field heating while its plasmonic nature would also not perturb the plasmonic resonance of the rod sufficiently enough to significantly change the resonance. The models (Fig. 4) did show the former spatial extension of the maximum electric field intensity to be true: the TiN-coated Au nanorods show a minimal electric field intensity at the edge of the Au and inside the coating film with the peak found at the outside edge of the TiN coating. The model also showed that the wavelength of maximum electric field intensity tends to red-shift from a 712 nm peak resonance when uncoated to ~830–930 nm for TiN PEALD coatings that are 2 nm thick and/or deposited at 90 °C with the presence of the TiN coating dampening the resonance intensity by >10× leading to a lower electric field intensity surrounding the nanorod (Fig. 4). Interestingly, the 90 °C 2 nm [1] sample shows a higher resonant field than the uncoated Au nanorod in the NIR,
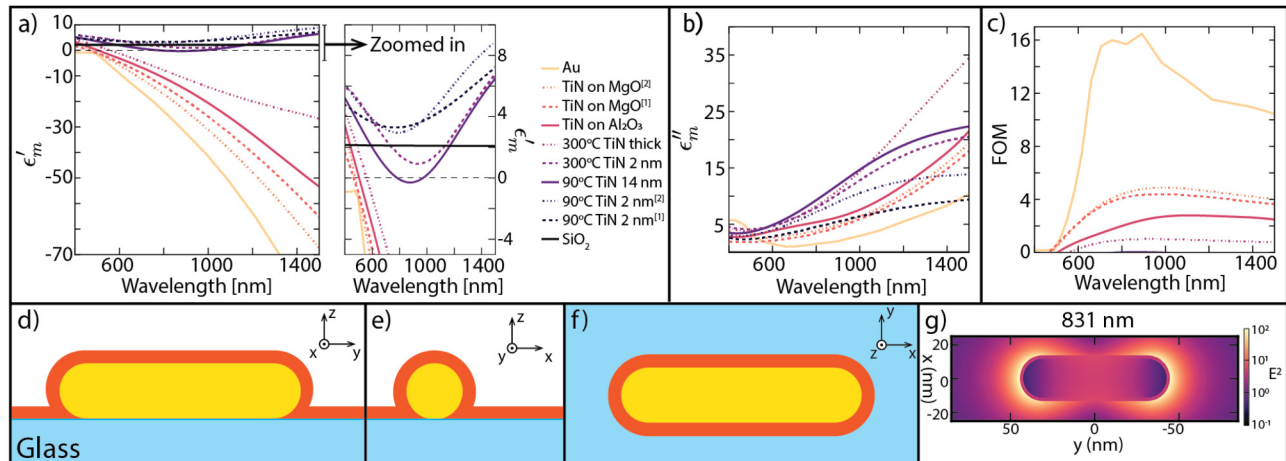
FIG. 3. Optical properties needed for simulation include the real (a) and imaginary (b) parts of the dielectric function of the various TiN films being used in this study along with the standard values for SiO₂, their ratio being the figure of merit (FOM) (c). In (a), it can be seen that the 90 °C deposited TiN films are either not plasmonic (both 2 nm films) or are barely able to exhibit any insignificant plasmonic behavior (the 14 nm film), which is also true for the 300 °C deposited 2 nm thick TiN film. The only PEALD TiN film demonstrating notable plasmonic behavior was the thick film deposited at 300 °C. The modeling design was constructed to include a Au nanorod positioned on a glass substrate where the nanorod also contained a 2 nm outer layer with optical properties that were varied in each model [(d)–(f)]. (g) The electric field intensity of a Au nanorod coated with 2 nm of 90 °C TiN 2 nm [1] is shown for comparison with the model schematics.

which may be due to the small imaginary part of its dielectric function [Fig. 3(b)]. Conversely, the higher-FOM TiN samples from Guler *et al.* tend to blue-shift the nanorod's resonance in a manner comparable to if the Au nanorod itself had become larger but with a different aspect ratio (89 nm full length, 27 nm diameter), but this still resulted in a peak resonance electric field intensity drop of >6×. Such a large shift and decrease in resonant intensity caused by any of the TiN coatings will be incompatible for an industrial technology with many other parameters to optimize like HAMR.[2,3,27] These results demonstrate that the plasmonic quality of the modeled PEALD TiN was not sufficiently matched to that of Au for maintaining the plasmonic quality and capability of the Au nanorods and instead likely became like any typical material with a different refractive index being detected by the plasmonic Au nanorod. While the match between Au and the Guler *et al.* TiN was better, it still has a parasitic effect on the resonance of the Au nanorod. As expected, the 2 nm SiO₂ coating yields a more modest red-shift to 745 nm, and the thicker 4.9 nm coating red-shifts the resonance to 781 nm, with a far lower drop in intensity. Interestingly, the intensity at the outside edge of the SiO₂ is greater than that of the Au nanorod 2 or 4.9 nm from its edge, meaning that the field in this region is enhanced by the SiO₂ and is ideal as a spacer if a coating is needed. Given our results, it does appear that a minimal imaginary part of the dielectric function is ideal, which is found in dielectric materials. This finding would strongly suggest that the plasmonic community can further its development efforts of Au high power density plasmonic devices using ultrathin coatings of dielectric ceramic materials rather than pursuing conductive ceramic options. ALD-based methods for depositing such materials will remain highly relevant. A dielectric material with good adhesion to Au would also serve the community well.

Nevertheless, there are many technical takeaways that will aid future directions beyond the scope of this work. TiN is an interesting material to study for such an application, but for reasons that go beyond plasmonics, it may not be an ideal candidate for the HAMR technology. TiN has been shown to oxidize in non-hermetically sealed environments ≳150–200 °C,[28,29] and these conditions would be relevant to HAMR drives under operation since the plasmonic antenna in the heads could reach these temperatures.[2,8] If a high-quality plasmonic TiN were achieved and used in the antenna near any possible contamination or less stable material containing oxygen, it is possible or even probable that its quality could be degraded during drive operation leading to possible failure. For this reason, it may be useful to explore possible plasmonic oxides with the same application concept demonstrated here. ReO₃ stands out as a possibility for applications up to 400 °C (where it converts to another oxidation state),[30–35] but it does not appear to be readily manufactured using any current semiconductor processing equipment. ALD-based methods are ideal for applying ultrathin conformal coatings, but Re has many oxidation states, so achieving the desired plasmonic oxidation state will be a challenge, not to mention that it will require a high-quality capable metal precursor to be developed for its ALD processing.[36,37] Still, we investigate ReO₃ here in Figs. 5(a)–5(d) but find similar results as we did with TiN. Furthermore, the HDD community has also described the drive failures due to the plasmonic antenna's properties as an issue with the further densification of the Au at its operating temperatures, which causes the antenna (and its high intensity near-field) to recess away from the surface and the magnetic media.[2] Finding methods for depositing Au in a denser manner or materials that act as surface adhesive layers (again without significantly interrupting the near-field) could be possible
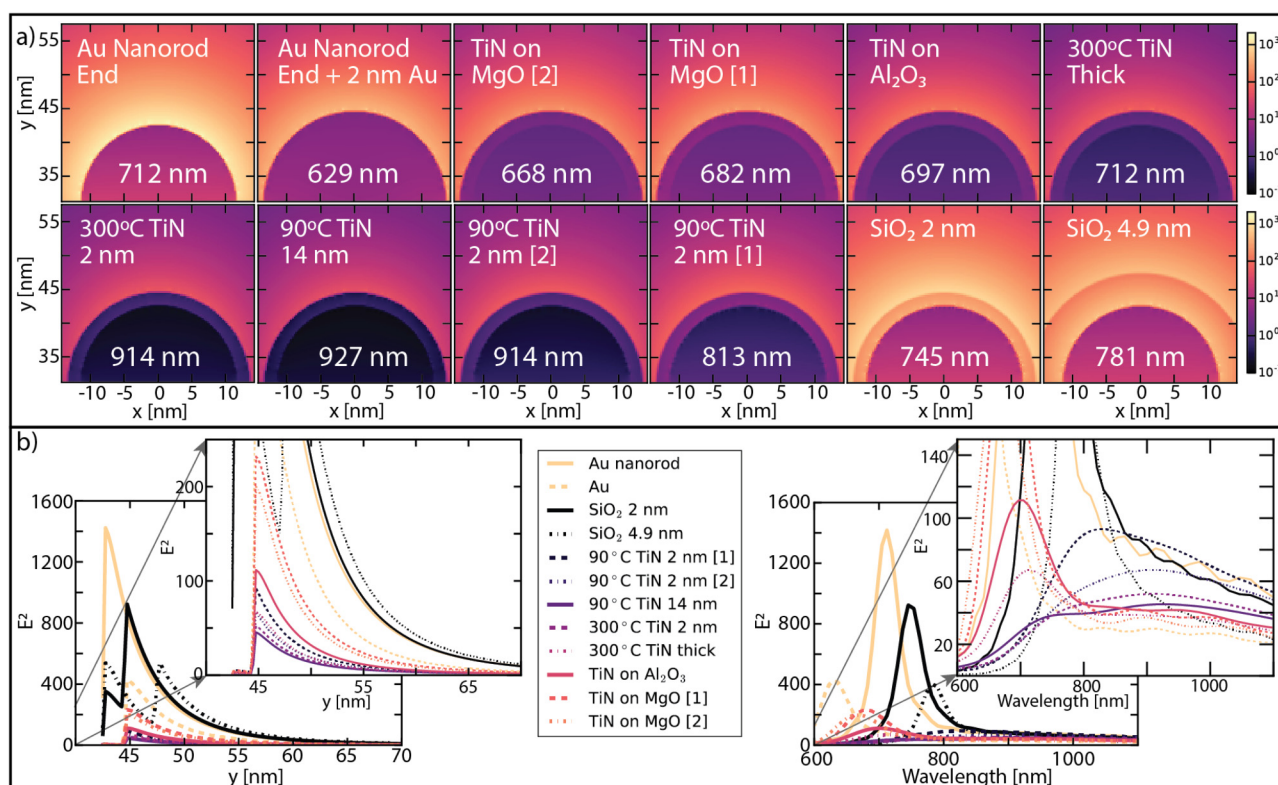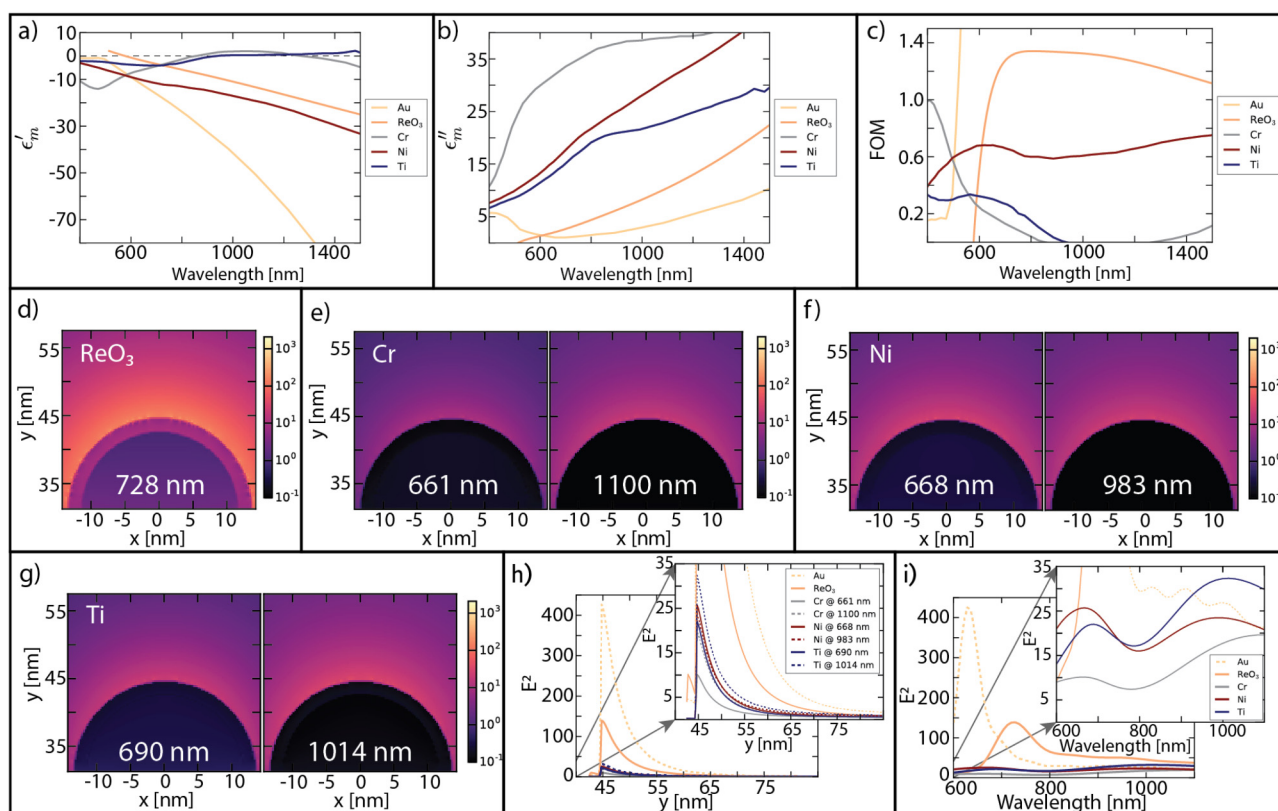
FIG. 4. (a) The maximum electric field intensity of coated and uncoated Au nanorods is shown at the tip of the rod for many conditions with the resonant wavelength listed at the top of each plot. All plots in part (a) are normalized to the upper left plot with the original nanorod dimensions without any additional coating. The white font indicates what coating is being modeled on the Au nanorod. For example, "TiN on MgO [2]" is a 2 nm film on the Au nanorod modeled with the dielectric function extracted from Guler *et al.*[15] and labeled "TiN (MgO) [2]" in that paper. Samples "As another example, '300C TiN Thick' is a 2 nm film on the Au nanorod modeled with the dielectric function extracted from Otto *et al.*[6,45] at its full thickness whereas '300C TiN 2 nm' is a 2 nm film on the Au nanorod modeled with the dielectric function extracted from Otto *et al.* at the point where the *in situ* measurements show that the film is 2 nm thick on the way to completing 2250 cycles and a thick film." The optical properties used for TiN films thicker than 2 nm were applied in the model as 2 nm layers to demonstrate limiting case scenarios. (b) Plots of the electric field intensity along the long axis of the nanorod (parallel to the y axis and at x = 0 and z = 11.5 nm) show direct comparisons of the electric field intensity at the respective resonance wavelengths where it can be seen that the original resonance is overall diminished by any of the coatings, but the strength of the resonance is modestly pushed out into space by the dielectric SiO_2 coatings. Plots of the electric field intensity vs the wavelength show the resonance position and shape for each coating scenario.

fixes, and TiN has previously been discussed as an option.[2,11,12] These adhesion layers include the metals Cr, Ni, Ti, and combinations thereof, with the pure metals being modeled again as 2 nm coatings on Au nanorods as shown in Fig. 5 with dielectric function data for Cr, Ni, and Ti taken from Palik[38] and ReO₃ taken from Weaver and Lynch.[32]

The semiconductor industry, adjacent in technology consumption and production, has been working to solve similar issues with nanoscale metals used in the initial interconnect layers in complementary metal oxide semiconductor (CMOS) chips for some time. Widely used Cu with TaN barriers has become insufficient at <10 nm dimensions due to the issues with fabricating high-quality copper at small dimensions and the lower conductivity of the conductive ceramic TaN barrier layer.[39] Researchers in this industry have explored and utilized Cu alloys and other metals such as Co, Ru, etc., together with little-to-no barrier layers, and

barrier layers or full interconnects comprised of a ternary carbide or nitride ceramic blend including a transition metal like Ti, an alloy metal like Si or Sn, and either C or N.[39–44] Theoretical modeling of such materials is guiding their explorative process and could potentially also yield solutions applicable to plasmonics if sufficiently conductive and band-structured materials are found. Finally, the TiN presented here (high and low temperatures) was not of optimal quality primarily due to the shared nature of the PEALD used and the oxide-containing films deposited previously contributing to the TiN's contamination and lower plasmonic behavior.[6,26,45] Furthermore, it is believed that the lower temperature deposited TiN is primarily amorphous while the higher temperature deposited TiN is primarily nanocrystalline and demonstrates more plasmonic behavior than the former.[26] Members of the ALD community have sought to improve the quality of its nitride materials deposited with plasma sources, and

FIG. 5. Optical properties needed for simulation include the real (a) and imaginary (b) parts of the dielectric function of the various Au adhesion layer films (and ReO₃) being used in this study, their ratio being the figure of merit (FOM) (c). (d)–(g) The maximum electric field intensity of coated Au nanorods is shown at the tip of the rod for several conditions with the resonant wavelength listed at the top of each plot. All plots in part (d)–(g) are normalized to the upper left plot in Fig. 4(a) having the original nanorod dimensions without any additional coating. (h) Plots of the electric field intensity along the long axis of the nanorod (parallel to the y axis and ax $x = 0$ and $z = 11.5$ nm) show direct comparisons of the electric field intensity at the respective resonance wavelengths where it can be seen that the original resonance is overall diminished by any of the coatings but least diminished by the ReO₃ coating. (i) Plots of the electric field intensity vs the wavelength show the resonance position and shape for each coating scenario.

chambers that are exclusively used for nitrides can still have oxygen contamination issues. Most PEALD systems use an inductively coupled plasma (ICP) system, which contains a ceramic material that can be a getter for water or oxygen, which would then be enveloped into the composition of nitride films during deposition.[46] Hollow cathode plasma (HCP) sources have proven to be useful for eliminating this contamination source in nitrides due to their all-metal design and could be used to improve the PEALD TiN properties and make the ultrathin films more conductive and plasmonic than currently achievable with other ALD approaches.[47] Still, TiN will not be sufficiently plasmonic or chemically stable enough to provide application to HAMR near the plasmonic antenna. Instead, the community should focus on dielectric ceramics as a morphologically stabilizing coating that minimize negative impact on plasmonic resonance and other related quality factors. Material adhesion to Au would also be highly beneficial.

In conclusion, we have explored the concept of using a PEALD TiN ultrathin coating to form a metal–ceramic composite plasmonic structure with a Au plasmonic antenna for the purposes of improving its thermal structural stability while maintaining its plasmonic properties near the surface, both of which are challenges for high power density plasmonics. Our proof-of-concept experiments showed that ultrathin layers of ceramic material were indeed useful for preserving the test-case Au nanorods' morphology, but our proof-of-concept electromagnetic field modeling showed significant changes in the resonance position and intensity that would be highly unfavorable for plasmonic antenna application. We followed these findings with a thorough discussion on other possible directions to look for solutions including plasmonic oxides, Au metal adhesion layers, and SiO₂, the latter appearing to be the best option.

METHODS

Nanorod deposition onto substrate

Silicon prime wafers (p type, $\langle 100 \rangle$) were cut into 1×1 cm² dimensioned squares (coupons) and coated with 0.1 w/v. % aqueous

poly-L-lysine, a positively charged amino acid polymer, solution (Sigma Aldrich) to enhance electrostatic adhesion between nanorods and substrate, followed by deposition of 23 nm diameter, 85 nm long Au nanorods in 3 mM CTAB aqueous solution (Nanopartz A12-25-808-CTAB-DIH-25). Various methods of deposition of the poly-L-lysine and nanorod solutions were tested, including spin-coating, dip-coating, and drop-casting. Preliminary tests showed that the method of nanorod deposition affected nanorod density, with dip-coating (1–2 min) and drop-casting (10 μl) producing moderate and high density configurations, while spin-coating (10 μl, 1000 rpm) led to lower density configurations (< 10 nanorods in 1 μm^2 viewing area), which initially seemed most desirable for analyzing optical response of individual rods without collective resonance effects from adjacent rods. For reproducibility, deposition of poly-L-lysine was performed as closely as recommended by literature[4] (spin-coat 50 μl, 3000 rpm followed by 60 °C 5 min bake), and nanorods were sonicated for 5 min and deposited using the aforementioned spin-coating method, with N$_2$ drying between deposition steps. Under time-limiting situations, poly-L-lysine was deposited via dip-coating samples for 3–4 min followed by N$_2$ drying and nanorod deposition via dip-coating for 1–2 min.

PEALD coatings and ultrathin film characterization

Coupon preparation was followed by ceramic coating deposition using plasma-enhanced atomic layer deposition (PEALD) (Oxford Instruments FlexAL). The deposited coatings targeted varying thickness of 0.5, 1, 2, 4, 8 nm material, specifically TiN deposited at 90 °C and SiO$_2$ at 40 °C using our previously published techniques.[6,26,45,48] For each deposition, the prepared silicon coupons were placed around the edges of a 250 nm thermal silica-coated silicon p-type wafer so that the center of the wafer could be used for *in situ* spectroscopic ellipsometry (SE, J.A. Woollam Inc., M2000) for evaluating the film growth during deposition. *Ex situ* determination of the TiN ultrathin film properties were also performed on the flat films on silica-coated silicon using variable angle SE (VASE) for understanding of the air-exposed TiN films using a fitted Drude–Lorentz oscillator model. Deposited films measured *in situ* were found to be 0.43, 1.0, 1.5, 2.0, and 3.9 nm in thickness.

Proof-of-concept thermal stability tests

To perform the proof-of-concept thermal stability tests, the coated and uncoated Au nanorods were annealed at 100 °C increments ranging from 100 to 500 °C to simulate possible high operating temperatures of high power density plasmonic devices. Samples were annealed in a quartz tube furnace, which was pumped and purged for two cycles and set under an inert, atmospheric Ar 250 SCCM environment for 0.5 h at the specified temperature.[26,48]

Proof-of-concept plasmonic activity tests

Three-dimensional finite-difference time-domain (FDTD) simulation using Lumerical was the method chosen for proof-of-concept simulations of the metal–ceramic composite system. For all simulations, except the 4.9 nm test with SiO$_2$, a 2 nm conformal coating of material is applied to the nanorod as well as to the surface of the SiO$_2$ (Palik, included in Lumerical package) substrate (as is the case in practice with ALD). For the simulation with the uncoated Au nanorod (23 nm diameter, 85 nm full length with hemisphere capped ends), the coating layer is given the same refractive index (permittivity) as the medium above the nanorod, $n = 1$ ($\epsilon_m = 1$). The nanorod was centered at x = 0, y = 0, and z = 11.5 nm where the longitudinal axis of the nanorod was placed along the y axis. Simulations were performed with the electric field oscillation along the y axis giving x, y, and z axis boundary conditions of symmetric, anti-symmetric, and perfectly matched layers, respectively. The source was configured as a Bloch/periodic plane wave with amplitude = 1 injected along the z axis from the +z direction (above the nanorod in our models). The modeled wavelength range was set to 600–1100 nm, and 50 frequency points were used. The mesh size in the nanorod's region plotted herein is 0.25 nm in all three dimensions. The Au nanorod was simulated using a fit to data from Johnson and Christy internally available within Lumerical (as was the case for Ag).[22] Cr, Ni, and Ti data were also internally available in Lumerical and were derived from Palik.[38] All other coatings tested were sourced from data imported into Lumerical from our measurements, our previous work, or the previous work of others. In the former cases, our deposited films' dielectric functions were measured *in situ*. In the latter case, TiN from Guler *et al.*[15] and ReO$_3$ from Weaver and Lynch[32] were extracted using the WebPlotDigitizer (https://apps.automeris.io/wpd/) to gather a set of data points for ϵ'_m and ϵ''_m, which were then fit to a function in Excel, and new values were extracted at common data points for importing into Lumerical. Within Lumerical, the data are fit again for use in the model. The SiO$_2$ PEALD coating was fitted using the standard model available in the CompleteEASE software for the ellipsometer to determine its thickness, and so the output dielectric function data were also imported into Lumerical.

AUTHOR DECLARATIONS
Conflict of Interest

The authors have no conflicts to disclose.

Author Contributions

Lauren M. Otto: Conceptualization (equal); Data curation (lead); Formal analysis (lead); Funding acquisition (lead); Investigation (lead); Methodology (lead); Project administration (lead); Resources (lead); Software (equal); Supervision (lead); Visualization (equal); Writing – original draft (lead); Writing – review & editing (equal). **Stephanie E. Liu:** Data curation (supporting); Investigation (supporting); Methodology (supporting); Visualization (supporting); Writing – review & editing (supporting). **Rowena W. Ng:** Data curation (supporting); Investigation (supporting); Writing – review & editing (supporting). **Adam M. Schwartzberg:** Funding acquisition (supporting); Investigation (supporting); Methodology (supporting); Resources (supporting); Supervision (supporting); Visualization (equal); Writing – review & editing (supporting). **Shaul Aloni:** Funding acquisition (supporting); Investigation (supporting); Project administration (supporting); Resources (supporting); Supervision (supporting). **Aeron Tynes Hammack:** Conceptualization (equal); Funding acquisition (supporting); Investigation (supporting); Methodology (supporting); Resources (supporting); Visualization (supporting); Writing – review & editing (supporting).

DATA AVAILABILITY

The data that support the findings of this study are available from the corresponding author upon reasonable request.

REFERENCES

[1]L. Gui, S. Bagheri, N. Strohfeldt, M. Hentschel, C. M. Zgrabik, B. Metzger, H. Linnenbank, E. L. Hu, and H. Giessen, Nano Lett. **16**, 5708 (2016).
[2]M. C. Kautzky and M. G. Blaber, MRS Bull **43**, 100 (2018).
[3]J. D. Kiely, P. M. Jones, and J. Hoehn, MRS Bull **43**, 119 (2018).
[4]W. A. Challener, C. Peng, A. V. Itagi, D. Karns, W. Peng, Y. Peng, X. Yang, X. Zhu, N. J. Gokemeijer, Y.-T. Hsia, G. Ju, R. E. Rottmayer, M. A. Seigler, and E. C. Gage, Nat. Photonics **3**, 220 (2009).
[5]B. C. Stipe, T. C. Strand, C. C. Poon, H. Balamane, T. D. Boone, J. A. Katine, J.-L. Li, V. Rawat, H. Nemoto, A. Hirotsune, O. Hellwig, R. Ruiz, E. Dobisz, D. S. Kercher, N. Robertson, T. R. Albrecht, and B. D. Terris, Nat. Photonics **4**, 484 (2010).
[6]L. M. Otto, A. T. Hammack, S. Aloni, D. Frank Ogletree, D. L. Olynick, S. Dhuey, B. J. H. Stadler, and A. M. Schwartzberg, Proc. SPIE **9919**, 99190N (2016).
[7]M. H. Kryder, E. C. Gage, T. W. McDaniel, W. A. Challener, R. E. Rottmayer, G. Ju, Y.-T. Hsia, and M. F. Erden, Proc. IEEE **96**, 1810 (2008).
[8]A. Kinkhabwala, M. Staffaroni, O. Suzer, S. Burgos, and B. Stipe, IEEE Trans. Magn. **52**, 1 (2016).
[9]T. Zhao, M. C. Kautzky, W. A. Challener, and M. A. Seigler, U.S. patent 20130235707A1 (31 October 2017).
[10]O. Mosendz, V. P. S. Rawat, and D. K. Weller, U.S. patent 9443545B2 (6 December 2016).
[11]Y. Cheng, T. Zhao, M. C. Kautzky, E. F. Rejda, K. W. Wierman, S. Franzen, A. J. Boyne, M. A. Seigler, and S. Jayashankar, U.S. patent 20150380020A1 (24 October 2017).
[12]X. Bian, Q. Dai, A. C. Lam, and B. C. Stipe, 9852749B2 (6 February 2020).
[13]U. Guler, A. Boltasseva, and V. M. Shalaev, Science **344**, 263 (2014).
[14]A. Boltasseva and V. M. Shalaev, Science **347**, 1308 (2015).
[15]U. Guler, A. V. Kildishev, A. Boltasseva, and V. M. Shalaev, Faraday Discuss. **178**, 71 (2015).
[16]G. V. Naik, B. Saha, J. Liu, S. M. Saber, E. A. Stach, J. M. K. Irudayaraj, T. D. Sands, V. M. Shalaev, and A. Boltasseva, Proc. Natl. Acad. Sci. U.S.A. **111**, 7546 (2014).
[17]G. V. Naik, V. M. Shalaev, and A. Boltasseva, Adv. Mater. **25**, 3264 (2013).
[18]C. M. Zgrabik and E. L. Hu, Opt. Mater. Express **5**, 2786 (2015).
[19]H. Wang, Q. Chen, L. Wen, S. Song, X. Hu, and G. Xu, Photonics Res. **3**, 329 (2015).
[20]A. A. Hussain, B. Sharma, T. Barman, and A. R. Pal, ACS Appl. Mater. Interfaces **8**, 4258 (2016).
[21]W. He, K. Ai, C. Jiang, Y. Li, X. Song, and L. Lu, Biomaterials **132**, 37 (2017).
[22]P. B. Johnson and R. W. Christy, Phys. Rev. B **6**, 4370 (1972).
[23]N. Zhou, X. Xu, A. T. Hammack, B. C. Stipe, K. Gao, W. Scholz, and E. C. Gage, Nanophotonics **3**, 141 (2014).
[24]X. Liu, D. Mazumdar, W. Shen, B. D. Schrag, and G. Xiao, Appl. Phys. Lett. **89**, 023504 (2006).
[25]D. Mazia, G. Schatten, and W. Sale, J. Cell Biol. **66**, 198 (1975).
[26]L. M. Otto, *Engineering Materials and Characterization Methods for Mass-Produced Plasmonic Devices* (University of Minnesota, 2017).
[27]K. Hono, Y. K. Takahashi, G. Ju, J.-U. Thiele, A. Ajan, X. Yang, R. Ruiz, and L. Wan, MRS Bull **43**, 93 (2018).
[28]Z. H. Cen, B. X. Xu, J. F. Hu, R. Ji, Y. T. Toh, K. D. Ye, and Y. F. Hu, J. Phys. D: Appl. Phys. **50**, 075105 (2017).
[29]N. C. Saha and H. G. Tompkins, J. Appl. Phys. **72**, 3072 (1992).
[30]A. Ferretti, D. B. Rogers, and J. B. Goodenough, Solid State Commun. **3**, lxxvii (1965).
[31]L. F. Mattheiss, Phys. Rev. **181**, 987 (1969).
[32]J. H. Weaver and D. W. Lynch, Phys. Rev. B **6**, 3620 (1972).
[33]K. Biswas and C. N. R. Rao, J. Phys. Chem. B **110**, 842 (2006).
[34]S. Ghosh, K. Biswas, and C. N. R. Rao, J. Mater. Chem. **17**, 2412 (2007).
[35]A. Agrawal, S. H. Cho, O. Zandi, S. Ghosh, R. W. Johns, and D. J. Milliron, Chem. Rev. **118**, 3121 (2018).
[36]J. Hämäläinen, K. Mizohata, K. Meinander, M. Mattinen, M. Vehkamäki, J. Räisänen, M. Ritala, and M. Leskelä, Angew. Chem. Int. Ed. **57**, 14538 (2018).
[37]S. Cwik, K. N. Woods, S. S. Perera, M. J. Saly, T. J. Knisley, and C. H. Winter, Dalton Trans. **50**, 18202 (2021).
[38]E. D. Palik, *Handbook of Optical Constants* (Academic Press Inc., 1985).
[39]D. C. Edelstein, in *2017 IEEE International Electron Devices Meeting (IEDM)* (IEEE, 2017), pp. 14.1.1–14.1.4.
[40]K. Sankaran, K. Moors, S. Dutta, C. Adelmann, Z. Tokei, and G. Pourtois, in *IEEE International Interconnect Technology Conference (IITC), 4–7 June 2018, Santa Clara, CA* (IEEE, New York, 2018), pp. 160–162.
[41]C. Adelmann, K. Sankaran, S. Dutta, A. Gupta, S. Kundu, G. Jamieson, K. Moors, N. Pinna, I. Ciofi, S. Van Eishocht, J. Bommels, G. Boccardi, C.J. Wilson, G. Pourtois, and Z. Tokei, *2018 IEEE International Interconnect Technology Conference (IITC)* (IEEE, 2018).
[42]C. Adelmann, L. G. Wen, A. P. Peter, Y. K. Siew, K. Croes, J. Swerts, M. Popovici, K. Sankaran, G. Pourtois, S. Van Elshocht, J. Bommels, and Z. Tokei, in *IEEE International Interconnect Technology Conference* (IEEE, 2014), pp. 173–176.
[43]K. Sankaran, S. Clima, M. Mees, C. Adelmann, Z. Tokei, and G. Pourtois, in *IEEE International Interconnect Technology Conference* (IEEE, 2014), pp. 193–196.
[44]K. Sankaran, S. Clima, M. Mees, and G. Pourtois, ECS J. Solid State Sci. Technol. **4**, N3127 (2015).
[45]L. M. Otto, A. T. Hammack, S. Aloni, D. Frank Ogletree, D. L. Olynick, S. D. Dhuey, B. J. H. Stadler, and A. M. Schwartzberg, Proc. SPIE **9919**, 991918 (2020).
[46]K. S. A. Butcher, M-P. F. Wintrebert, P. P.-T. Chen, J. L. P. Ten Have, and D. I. Johnson, 8298624B2 (30 October 2012).
[47]K. S. A. Butcher, D. Alexandrov, P. Terziyska, V. Georgiev, and D. Georgieva, Phys. Status Solidi C **9**, 1070 (2012).
[48]L. M. Otto, E. A. Gaulding, C. T. Chen, T. R. Kuykendall, A. T. Hammack, F. M. Toma, D. F. Ogletree, S. Aloni, B. J. H. Stadler, and A. M. Schwartzberg, Sci. Rep. **11**, 7656 (2021).